Hydrogenation of acetylene and propyne over hydrogen storage ErNi5-xAlx?alloys and the role of absorbed hydrogen

doi: 10.1016/j.ijhydene.2020.05.062

Revised manuscript: HE-D-20-00609R1 (Clean)

Hydrogenation of acetylene and propyne over hydrogen storage $ErNi_{5-x}Al_x$ alloys and the role of absorbed hydrogen.

Ryota Tsukuda[a,b], Takayuki Kojima[a,c], Daisuke Okuyama[a], Satoshi Kameoka[a], Chikashi Nishimura[d], An-Pang Tsai[a,d]

[a] Institute of Multidisciplinary Research for Advanced Materials, Tohoku University, Katahira 2-1-1, Aoba-ku, Sendai, 980-8577, Japan

[b] Department of Materials Processing, Graduate School of Engineering, Tohoku University, Aoba-yama 6-6-02, Aoba-ku, Sendai, 980-8579, Japan

[c] Frontier Research Institute for Interdisciplinary Sciences, Tohoku University, Aramaki Aza Aoba 6-3, Aoba-ku, Sendai, 980-8578, Japan

[d] National Institute for Materials Science, Sengen 1-2-1, Tsukuba, 305-0047, Japan

Highlights

- The hydrogen storage properties of $ErNi_{5-x}Al_x$ alloys were studied at temperatures higher than 25 °C.
- Hydrogen absorbed in $ErNi_{3.5}Al_{1.5}$ improved the catalytic activity for the

hydrogenation of acetylene and propyne.

- The contribution of absorbed hydrogen to hydrogenation is discussed with respect to transient response and pulse tests.
- The hydrogen absorbed in $ErNi_{3.5}Al_{1.5}$ plays important roles in the activation of C_2H_2 and H_2.

Graphical abstract

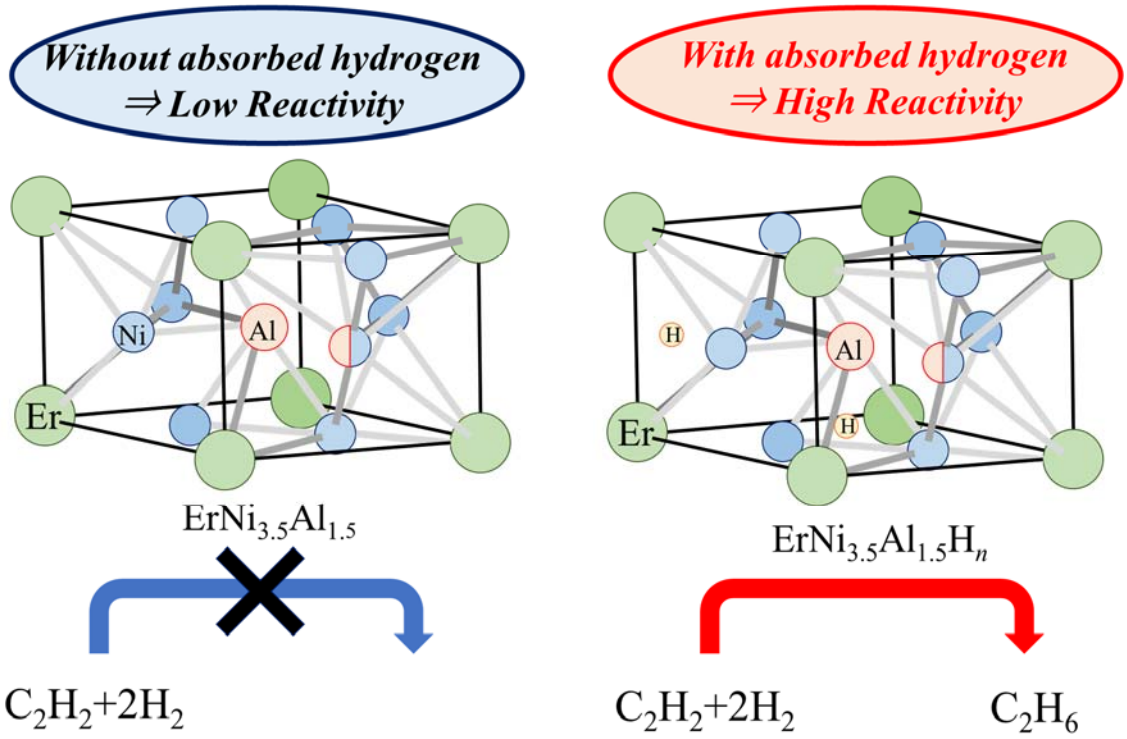

Keywords

Intermetallic compounds; Hydrogen storage alloys; $ErNi_{5-x}Al_x$ alloys; Hydrogenation of alkynes; Activity of absorbed hydrogen

Abstract

The hydrogen storage properties of $ErNi_{5-x}Al_x$ (x=0, 0.5, 0.75, 1, 1.25, and 1.5) alloys were investigated by pressure-composition isotherms and *in situ* X-ray diffraction measurements under a hydrogen atmosphere. Catalytic reactivities toward the hydrogenation of alkynes (acetylene and propyne) over $ErNi_{5-x}Al_x$ (x=0, 1, and 1.5) alloys were also studied and the contribution of absorbed hydrogen to hydrogenation is discussed. All $ErNi_{5-x}Al_x$ alloys possess a hexagonal structure ($CaCu_5$-type) with the space group P6/mmm. The substitution of Al for Ni facilitated hydrogen absorption at lower hydrogen pressures by the formation of larger interstitial spaces. $ErNi_{3.5}Al_{1.5}H_n$ with absorbed hydrogen showed higher reactivities for the catalytic hydrogenation of acetylene and propyne than $ErNi_5$ and $ErNi_4Al$ without absorbed hydrogen. The reason for this was concluded to be that absorbed hydrogen activates adsorbates (C_2H_2 and hydrogen) that are supplied from the gas phase.

1. Introduction

Hydrogen is an ideal energy resource because of its portability and low environmental influence. Hydrogen storage is an important technology to make hydrogen available for use. Development of the properties of many hydrogen storage alloys has been reported, such as hydrogen capacity, and kinetic and cyclic behavior [1-3]. $RENi_5$ (RE= rare earth) type alloys, *e.g.* $LaNi_5$, are well-known hydrogen storage alloys. The advantages of these alloys are their high hydrogen absorption and desorption kinetics [4]. The substitution of Al for Ni changes the stability of the hydride, and the

hydrogen storage properties of many $RENi_{5-x}Al_x$ alloys (RE = La [5,6], Ce [7], Y [8], Nd, Gd [9], Sm [10], Tb [11], Dy [12], and Ho [13]) have been reported. The hydrogen storage capacities of $ErNi_{5-x}Al_x$ alloys (x=0.5, 1, and 1.5) measured by pressure-composition isotherm (PCI) have been reported [14]; however, the measurement temperature range is mostly lower than 25 °C and the hydrogen storage properties in higher temperature regions have not been reported. Furthermore, the structure of hydrides in $ErNi_{5-x}Al_x$ alloys has not been investigated, except for $ErNi_4AlH_n$ [15], even though understanding of the structure of hydrides and their formation processes is important for the development of hydrogen storage alloys. Therefore, the first purpose of this study is to examine detailed hydrogen storage properties of $ErNi_{5-x}Al_x$ alloys at temperatures higher than 25 °C and the structure of their hydrides by *in situ* X-ray diffraction (XRD) under a hydrogen atmosphere.

In addition, hydrogen storage alloys are expected to show high catalytic reactivity for the hydrogenation reaction because they provide reactants with hydrogen from a bulk alloy, which would be a new route that is different from the gas phase. The state of absorbed hydrogen supplied from a bulk alloy is similar to a dissociative hydrogen atom. Absorbed hydrogen would thus be effective for a catalytic reaction because there is no necessity to dissociate hydrogen molecules on the surface. Hydrogen absorbed in Pd is also important for the hydrogenation of hydrocarbons, as exemplified in many reports on Pd catalysts [16-23]. There have been some studies on hydrogen storage alloys for the catalytic hydrogenation of ethylene (C_2H_4) and carbon dioxide [24-28]. We recently reported that the hydrogenation of alkynes (C_nH_{2n-2}) over $RENi_5$-type hydrogen storage alloys, $CeNi_{5-x}(Al, Ga)_x$ alloys, and absorbed hydrogen in $CeNi_{5-x}(Al, Ga)_x$ alloys improves the catalytic reactivity toward the hydrogenation of C_nH_{2n-2} [7,29]. However,

the detailed contribution of absorbed hydrogen to the hydrogenation of C_nH_{2n-2} was not clear in previous reports [7,29], in that it was not revealed whether absorbed hydrogen reacts with C_nH_{2n-2} directly or absorbed hydrogen activates adsorbates (C_nH_{2n-2} or hydrogen). The second purpose of this study is to elucidate the role of absorbed hydrogen in the hydrogenation of C_nH_{2n-2}.

2. Experimental procedures

2.1. Material preparation

Pure Er, Ni, and Al were mixed in appropriate ratios to prepare a series of $ErNi_{5-x}Al_x$ alloys (x=0, 0.5, 0.75, 1, 1.25, and 1.5) in an arc-melting furnace under an Ar atmosphere. The elemental purities were Er 99.9%, Ni 99.99%, and Al 99.99%. The as-cast alloys were annealed at 800 °C for 72 h under an Ar atmosphere to achieve homogenization. The annealed samples were then sieved to <20 μm. Structural analysis and phase identification were conducted using powder XRD (Rigaku Ultima IV) with Cu Kα radiation. The XRD data were analyzed by the Rietveld method to calculate lattice parameters and to determine the substitution site of Al. The FULLPROF program was used to analyze the XRD data [30]. XRD calculations were based on the hexagonal crystal structure with the space group P6/mmm (No. 191).

2.2. Measurement of hydrogen storage properties

The hydrogen storage properties of $ErNi_{5-x}Al_x$ alloys (x=0, 0.5, 0.75, 1, 1.25, and

1.5) were investigated by the volumetric method using a standard Sieverts apparatus (Suzuki Shokan). The samples, sieved to a size in the range of 25–90 μm, were placed in a stainless vessel. Hydrogen gas was introduced into the vessel up to 3 MPa, followed by heating of the samples at 300 °C for 1 h as an initial activation process. After these pretreatments, PCI measurements were conducted at 25 °C, 75 °C, and 125 °C.

In situ XRD analyses of $ErNi_4Al$, $ErNi_{3.75}Al_{1.25}$, and $ErNi_{3.5}Al_{1.5}$ were performed at 25 °C and 75 °C (PANalytical, Empyrean). These powder samples were transferred into a silicon container and then kept at room temperature for 30 min under vacuum before being heated at 300 °C for 1 h under hydrogen pressure at 0.8 MPa, and finally cooled to the room temperature. The *in situ* XRD data were acquired during a desorption process under various hydrogen pressures at 25 °C and 75 °C.

2.3. Examination of catalytic activity

2.3.1. Constant flow test

Catalyst tests were conducted for $ErNi_5$, $ErNi_4Al$, and $ErNi_{3.5}Al_{1.5}$. These samples were sieved in the range of 25–90 μm. The catalyst tests were performed using a standard fixed-bed flow reactor. The samples were activated under a pure hydrogen flow of 0.1 MPa at 30 mL min^{-1} and heated at 300 °C for 1 h. The samples were then cooled to room temperature under the hydrogen flow. The reaction gases were 0.7% C_2H_2/6% He/93.3% H_2 (P_{H2} = 0.093 MPa) and 0.4% C_3H_4/19.6% He/80% H_2 (P_{H2} = 0.08 MPa). The total flow rates and pressures were fixed to 30 mL min^{-1} and 0.1 MPa, and 60 mL min^{-1} and 0.1 MPa, respectively. The products from the hydrogenation of C_2H_2 were

analyzed by in-line gas chromatography (GC; Shimadzu GC-8 A, thermal conductivity detector (TCD)) with a Shincarbon ST column using He as the carrier gas and those from the hydrogenation of C_3H_4 were detected using GC (Agilent 490 Micro GC, TCD) with a PoraPLOT Q column using He as the carrier gas. The conversion of C_nH_{2n-2} and selectivity toward alkenes (C_nH_{2n}) were defined as:

$$C_{CnH2n-2}\,[\%] = ([C_nH_{2n-2}(\text{feed})]_{mol} - [C_nH_{2n-2}]_{mol})/[C_nH_{2n-2}\,(\text{feed})]_{mol} \times 100, \quad (1)$$

$$S_{CnH2n}\,[\%] = [C_nH_{2n}]_{mol}/([C_nH_{2n}]_{mol} + [C_nH_{2n+2}]_{mol}) \times 100, \quad (2)$$

where $[C_xH_y]_{mol}$ and $[C_xH_y(\text{feed})]_{mol}$ represent the molar concentrations in the outlet gases and molar concentrations in the feed stream, respectively. The amount of carbon loss was defined as:

$$C_{loss}\,[\%] = ([C_nH_{2n-2}(\text{feed})]_{mol} - [C_nH_{2n-2}]_{mol} - [C_nH_{2n}]_{mol} - [C_nH_{2n+2}]_{mol})/[C_nH_{2n-2}\,(\text{feed})]_{mol} \times 100. \quad (3)$$

The catalytic activity was monitored every 15 min.

The surface areas of the powder catalysts were estimated using the Brunauer-Emmett-Teller (BET) method with Kr adsorption. The specific surface areas of specimens were: $ErNi_5$ 0.0896 $m^2\ g^{-1}$, $ErNi_4Al$ 0.0835 $m^2\ g^{-1}$, and $ErNi_{3.5}Al_{1.5}$ 0.0806 $m^2\ g^{-1}$.

2.3.2. Transient response tests

If hydrogen absorbed in a bulk alloy is consumed during catalytic reactions, then hydrogenation is considered to occur only with the flow of gaseous C_2H_2 and He, but without H_2 in the reaction gas. Therefore, transient response tests were conducted by alternating gaseous C_2H_2+He and C_2H_2+H_2 to reveal whether absorbed hydrogen alone

can drive hydrogenation in the absence of a hydrogen supply from the gas phase.

$ErNi_5$ and $ErNi_{3.5}Al_{1.5}$ sieved in the range of 25–90 μm were selected as samples for transient response tests. A similar transient response test was also conducted for $ErNi_{3.5}Al_{1.5}$ sieved to <20 μm to investigate the effect of the catalyst particle size. The specific surface area of $ErNi_{3.5}Al_{1.5}$ (<20 μm) estimated by the BET method was 0.468 $m^2\ g^{-1}$.

The initial activation process for each sample was the same as that for the catalytic test. Reaction gases of 0.7% C_2H_2/6% He/93.3% H_2 and 0.7% C_2H_2/99.3% He were switched alternately. The measurement temperature was 75 °C.

2.3.3. Pulse test

Pulse tests were performed to determine the contribution of absorbed hydrogen using $ErNi_{3.5}Al_{1.5}$ sieved from 25 μm to 90 μm as the specimen. Two different initial treatments were conducted for $ErNi_{3.5}Al_{1.5}$ and each specimen with/without absorbed hydrogen ($ErNi_{3.5}Al_{1.5}H_n$/$ErNi_{3.5}Al_{1.5}$) was produced differently. (1) $ErNi_{3.5}Al_{1.5}H_n$ was synthesized under a pure hydrogen flow of 0.1 MPa at 30 mL min^{-1} and heated at 300 °C for 1 h, after which it was cooled to room temperature and kept for 30 min under the hydrogen flow. (2) $ErNi_{3.5}Al_{1.5}$ without absorbed hydrogen was prepared under a hydrogen flow of 0.1 MPa at 30 mL min^{-1} and heated at 300 °C for 1 h, after which the hydrogen flow was switched to a He flow at the same flow rate. The sample was kept for 30 min at 300 °C under the He flow. The specimen was finally cooled down to room temperature and kept for 30 min under a He atmosphere.

The weight of each sample was ca. 0.32 g. The pulse tests were conducted after He

gas at 30 mL min^{-1} was flowed for 10 min to purge the reactor. The pulse gas used was 2% C_2H_2/18% He/80% H_2 or 2% C_2H_2/98% He, and the total pressure was 0.1 MPa. Pulse gas (1.34 mL) was injected into a He carrier gas at 30 mL min^{-1} and forwarded to the specimen in the pulse test. The second pulse gas was sent 15 min later after introduction of the first pulse gas. The measurement temperature was 25 °C.

3. Results and discussion

3.1. Structure of $ErNi_{5-x}Al_x$ (x=0, 0.5, 0.75, 1, 1.25, and 1.5) alloys

Fig. 1 shows XRD patterns for the series of $ErNi_{5-x}Al_x$ alloys. The XRD patterns show that all alloys possess the same hexagonal structure ($CaCu_5$-type) with the space group P6/mmm. Er atoms in $ErNi_5$ occupy vertices site (1*a* site) and the Ni atoms occupy two different atomic sites, the z = 0 plane (2*c* site) and the z = 1/2 plane (3*g* site), as shown in Fig. 2. Rietveld analysis indicated that all Al atoms occupy 3*g* sites, which is consistent with a previous report [14]. Table 1 shows the lattice parameters and unit cell volumes of $ErNi_{5-x}Al_x$ alloys determined by Rietveld analysis. The atomic radius of Al is larger than that of Ni; therefore, the unit cell volume increases with the Al content.

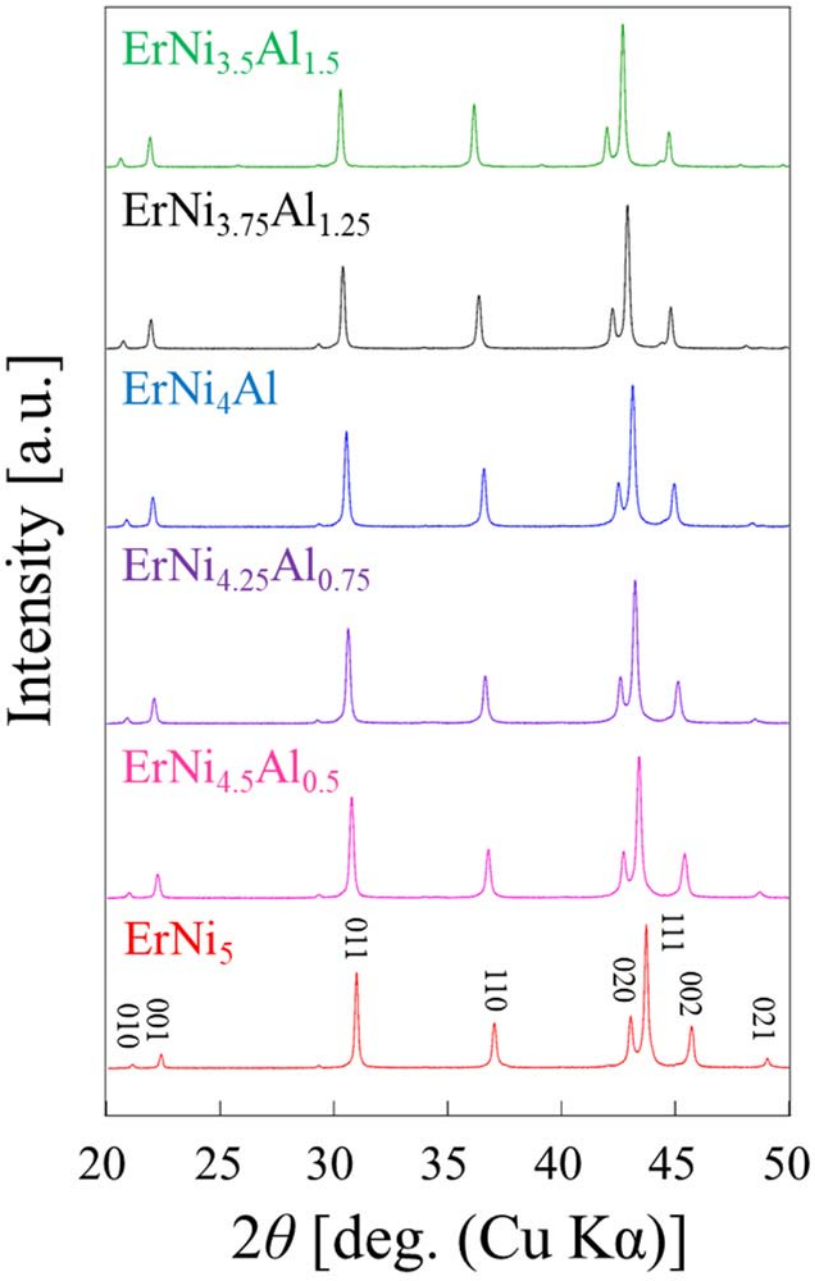

Fig. 1. XRD patterns for $ErNi_{5-x}Al_x$ (x=0, 0.5, 0.75, 1, 1.25, and 1.5) alloys.

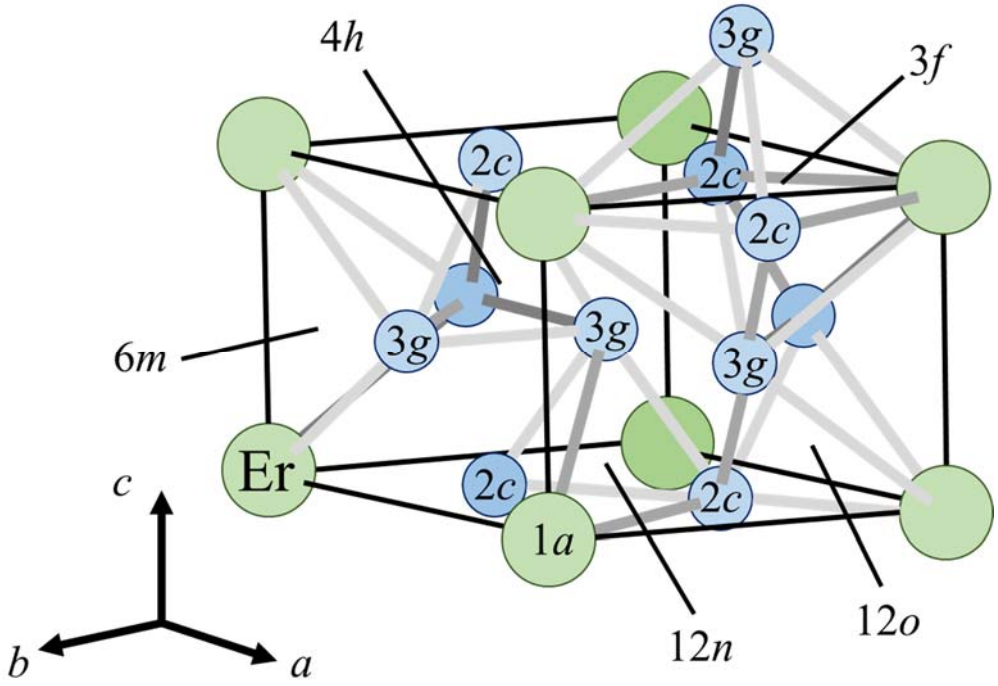

Fig. 2. Schematic diagram of the $CaCu_5$-type structure.

Table 1 Lattice parameters and unit cell volumes of the $ErNi_{5-x}Al_x$ alloys

Composition	*a*-axis [□]	*c*-axis [□]	Unit cell volume [□^{3}]	Reference
$ErNi_5$	4.854	3.970	81.00	This study
$ErNi_5$	4.866	3.977	81.55	[14]
$ErNi_5$	4.856	3.966	80.99	[31]
$ErNi_5$	4.854	3.964	80.88	[32]
$ErNi_{4.5}Al_{0.5}$	4.885	3.993	82.52	This study
$ErNi_{4.5}Al_{0.5}$	4.890	4.002	82.87	[14]
$ErNi_{4.25}Al_{0.75}$	4.898	4.014	83.40	This study
$ErNi_4Al$	4.910	4.032	84.17	This study
$ErNi_4Al$	4.910	4.034	84.22	[14]
$ErNi_4Al$	4.910	4.033	84.20	[15]
$ErNi_{3.75}Al_{1.25}$	4.935	4.042	85.26	This study
$ErNi_{3.5}Al_{1.5}$	4.963	4.049	86.37	This study
$ErNi_{3.5}Al_{1.5}$	4.966	4.062	86.75	[14]

3.2 Hydrogen storage properties of $ErNi_{5-x}Al_x$ (x=0, 0.5, 0.75, 1, 1.25, and 1.5)

All $ErNi_{5-x}Al_x$ (x=0, 0.5, 0.75, 1, 1.25, and 1.5) alloys were exposed to hydrogen gas under different pressures and temperatures to obtain PCIs. Fig. 3 shows the results of PCI measurements for the $ErNi_{5-x}Al_x$ (x=0, 0.5, 0.75, 1, 1.25, and 1.5) alloys. No equilibrium plateau pressure was observed at hydrogen pressures up to 4 MPa for $ErNi_5$ and $ErNi_{4.5}Al_{0.5}$ at 25–125 °C. The equilibrium plateau pressures for the $ErNi_{5-x}Al_x$ (x=0.75, 1, 1.25, and 1.5) alloys decreased with an increase in the Al content. These alloys absorb hydrogen at lower hydrogen pressures. $ErNi_{3.5}Al_{1.5}$ exhibits hydrogen storage capacity at hydrogen pressures near barometric pressure. The reason for this is that the substitution of Al for Ni facilitates hydrogen absorption because the replacement of Ni with Al creates larger interstitial spaces. The plateau pressure increased with the measurement temperature.

Fig. 4 shows *in situ* XRD patterns for $ErNi_{3.75}Al_{1.25}$ at 75 °C and various hydrogen pressures. The *in situ* XRD patterns reveal that the hydrides have the same index peaks of the matrix phase with the hexagonal structure. Two phases, $ErNi_{3.75}Al_{1.25}$ (matrix phase) and the hydride phase, are observed at 0.2 MPa in the plateau region [Fig. 3(e) at 0.2 MPa, 75 °C], as shown in Fig. 4. The variations in the lattice constants for each hydride are shown in Fig. 5 as a function of the hydrogen pressure. Expansion along the a-axis due to the hydrogen pressure is slightly longer than that along the c-axis (*e.g.* $\Delta a \leq 0.18$ Å, $\Delta a/a_0 \times 100 \leq 3.7\%$ up to 0.7 MPa H_2, and $\Delta c \leq 0.11$ Å, $\Delta c/c_0 \times 100 \leq 2.6\%$ up to 0.7 MPa H_2 in $ErNi_{3.75}Al_{1.25}$ at 25 °C). Similar anisotropic lattice expansion is observed in $RENi_5$-type alloys, such as $LaNi_4AlD_n$ [33] and $LaNi_{4.25}Al_{0.75}D_n$ [34]. These

neutron diffraction studies indicated that deuterium atoms selectively occupy the 6*m* and 12*n* sites [Fig. 2]. Therefore, hydrogen atoms in $ErNi_{5-x}Al_x$ alloys are presumed to occupy the 6*m* and 12*n* sites.

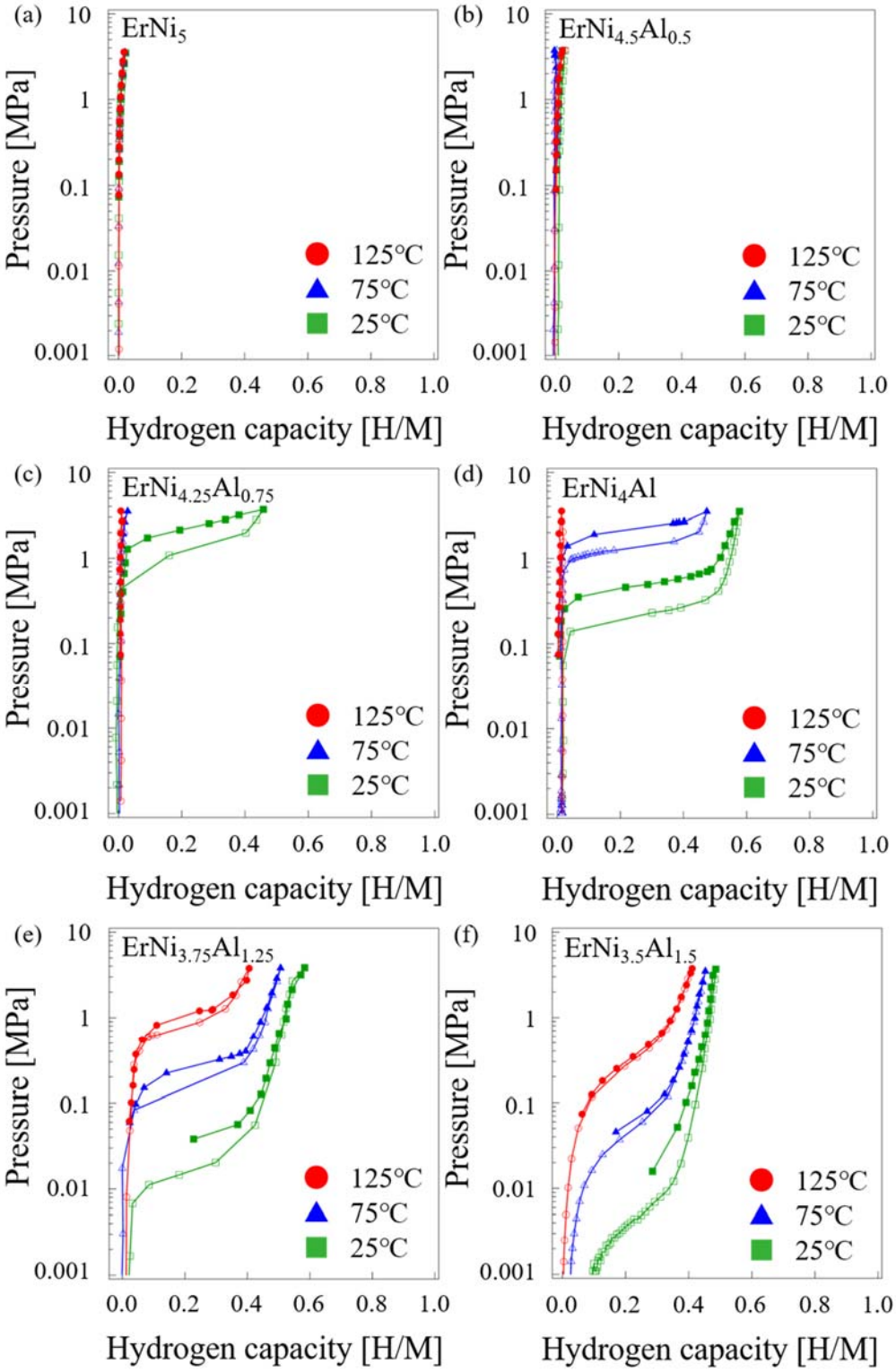

Fig. 3. PCI measurements for $ErNi_{5-x}Al_x$ alloys; (a) $ErNi_5$, (b) $ErNi_{4.5}Al_{0.5}$, (c) $ErNi_{4.25}Al_{0.75}$, (d) $ErNi_4Al$, (e) $ErNi_{3.75}Al_{1.25}$, and (f) $ErNi_{3.5}Al_{1.5}$.

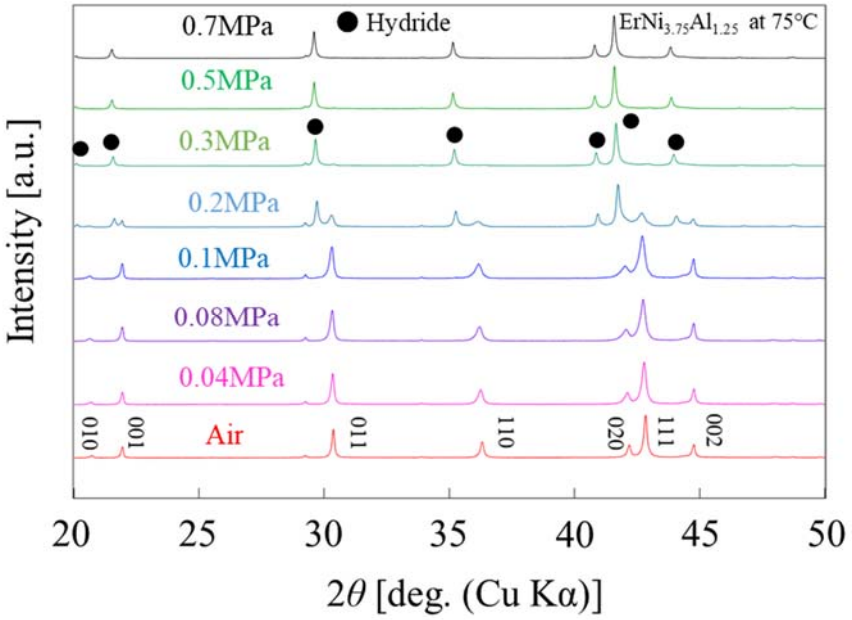

Fig. 4. *In situ* XRD patterns for $ErNi_{3.75}Al_{1.25}$ measured at 75 °C.

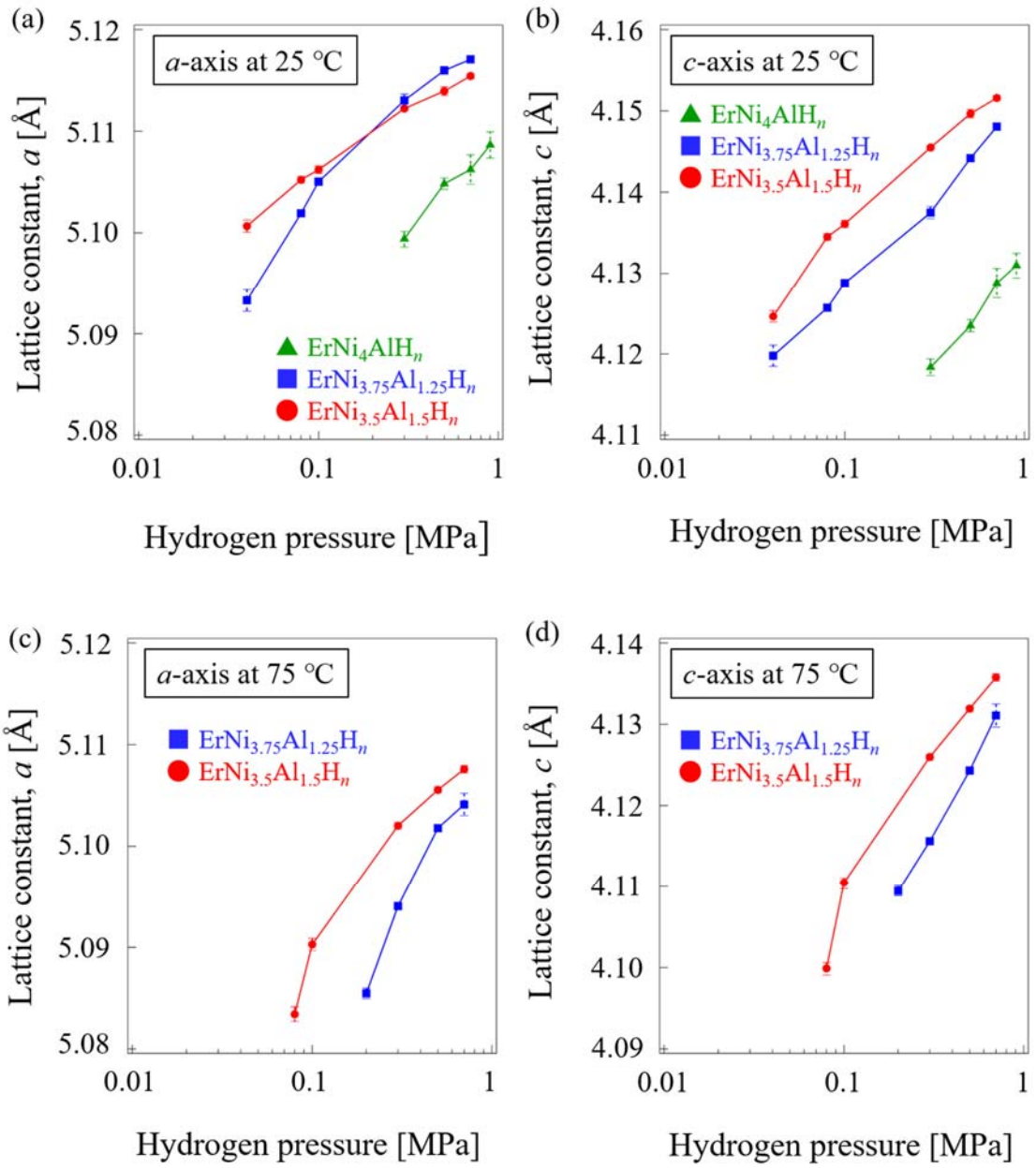

Fig. 5. Variation in lattice constants as a function of the hydrogen pressure for each hydride: (a) *a*-axis at 25 °C, (b) *c*-axis at 25 °C, (c) *a*-axis at 75 °C, (d) *c*-axis at 75 °C.

3.3 Hydrogenation of C_2H_2 and C_3H_4 in constant flow tests

Catalytic tests for the hydrogenation of C_2H_2 and C_3H_4 were conducted using three

samples, $ErNi_5$, $ErNi_4Al$, and $ErNi_{3.5}Al_{1.5}$. $ErNi_{3.5}Al_{1.5}$ was the only alloy able to absorb hydrogen under the measurement conditions (hydrogenation of C_2H_2 at P_{H2} = 0.093 MPa, hydrogenation of C_3H_4 at P_{H2} = 0.08 MPa) and form the hydride, $ErNi_{3.5}Al_{1.5}H_n$ [Fig. 3(f)]. $ErNi_5$ and $ErNi_4Al$ did not absorb hydrogen under the measurement conditions [Figs. 3(a) and (d)]. Conversion and selectivity for the hydrogenation of C_2H_2 are shown in Fig. 6. The weight of the specimens, surface areas and hydrogen storage capacities (P_{H2} = 0.093 MPa) are presented in Table 2. The surface area of each weighed sample was approximately 0.025 m^2.

$ErNi_5$ and $ErNi_4Al$ without absorbed hydrogen showed almost the same activity during catalytic tests [Fig. 6(a)]. Therefore, the substitution of Al is considered to have little effect under the measurement conditions. In contrast, $ErNi_{3.5}Al_{1.5}$ with absorbed hydrogen, $ErNi_{3.5}Al_{1.5}H_n$, showed higher reactivity for the hydrogenation of C_2H_2 than $ErNi_5$ and $ErNi_4Al$ at less than 75 °C, where absorbed hydrogen is present in the bulk of $ErNi_{3.5}Al_{1.5}$. The selectivity toward C_2H_4 over all the specimens decreased when the conversion reached 100%, and the product was almost all ethane (C_2H_6), as shown in Fig. 6(b). The amount of carbon deposit or higher hydrocarbons formation (*e.g.* C_4H_x) for each alloy was almost the same, *e.g.* C_{loss} was 4–11% at 75 °C and approximately 20–25% at 125 °C.

Similarly, the results for the hydrogenation of C_3H_4 are shown in Fig. 7. The weight of the specimens and their surface areas are presented in Table 3. $ErNi_{3.5}Al_{1.5}$ also absorbed hydrogen under the measurement conditions (P_{H2}=0.08 MPa). In contrast, $ErNi_5$ and $ErNi_4Al$ did not include absorbed hydrogen. $ErNi_5$ and $ErNi_4Al$ showed similar reactivity for the hydrogenation of C_3H_4 [Fig. 7(a)], whereas $ErNi_{3.5}Al_{1.5}H_n$ showed higher reactivity for the hydrogenation of C_3H_4 as with that for C_2H_2. The

selectivity toward propene (C_3H_6) over all the alloys decreased when all the C_3H_4 was converted and propane (C_3H_8) was produced, as shown in Fig. 7(b). The carbon loss for each specimen amounted to less than 9% at every measurement temperature.

These results indicate that hydrogen absorbed in $ErNi_{3.5}Al_{1.5}$ improves the catalytic reactivity for the hydrogenation of C_2H_2 and C_3H_4, as with previous reports on $CeNi_{5-x}(Al,Ga)_x$ alloys [7,29]. The increase in the conversion rate over $ErNi_5$ and $ErNi_4Al$ for the hydrogenation of C_2H_2 and C_3H_4 increased with the measurement temperature [Figs. 6(a) and 7(a)]. However, the conversion of C_2H_2 over $ErNi_{3.5}Al_{1.5}H_n$ decreased at 75 °C [Fig. 6(a)] and the increase in the conversion of C_3H_4 is gentle between 50 °C and 75 °C [Fig. 7(a)]. This seems to be due to the reduction of absorbed hydrogen in $ErNi_{3.5}Al_{1.5}H_n$. The improvement in conversion with absorbed hydrogen may decrease with an increase in the temperature because the hydrogen storage capacity decreases with an increase in the temperature, as shown in Table 2.

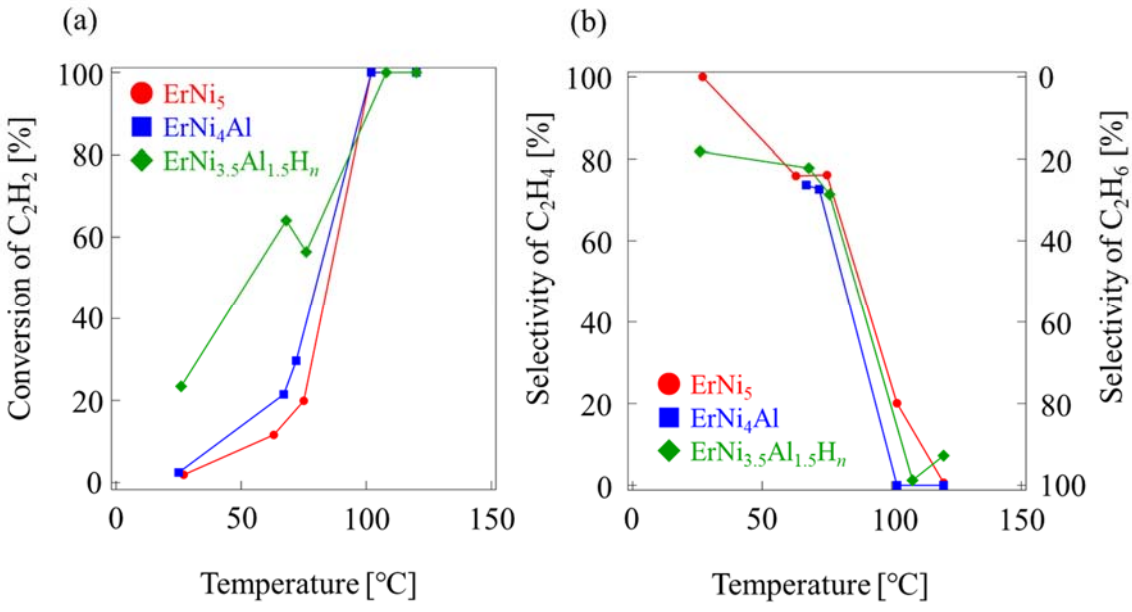

Fig. 6. (a) Conversion of C_2H_2 and (b) selectivity toward C_2H_4 over $ErNi_5$, $ErNi_4Al$, and

$ErNi_{3.5}Al_{1.5}$ (reaction gas: 0.7% C_2H_2/6% He/93.3% H_2, total pressure: 0.1 MPa, flow rate: 30 mL min^{-1}).

Table 2 Weight, surface area and hydrogen capacity at P_{H2} = 0.093 MPa of each $ErNi_{5-x}Al_x$ alloy in the hydrogenation of C_2H_2

Sample	Weight [g]	Surface area [m^2]	Hydrogen capacity	
			25 □ [H/M]	75 □ [H/M]
$ErNi_5$	0.2835	0.0254	0	0
$ErNi_4Al$	0.3082	0.0258	0	0
$ErNi_{3.5}Al_{1.5}H_n$	0.3220	0.0260	0.38	0.28

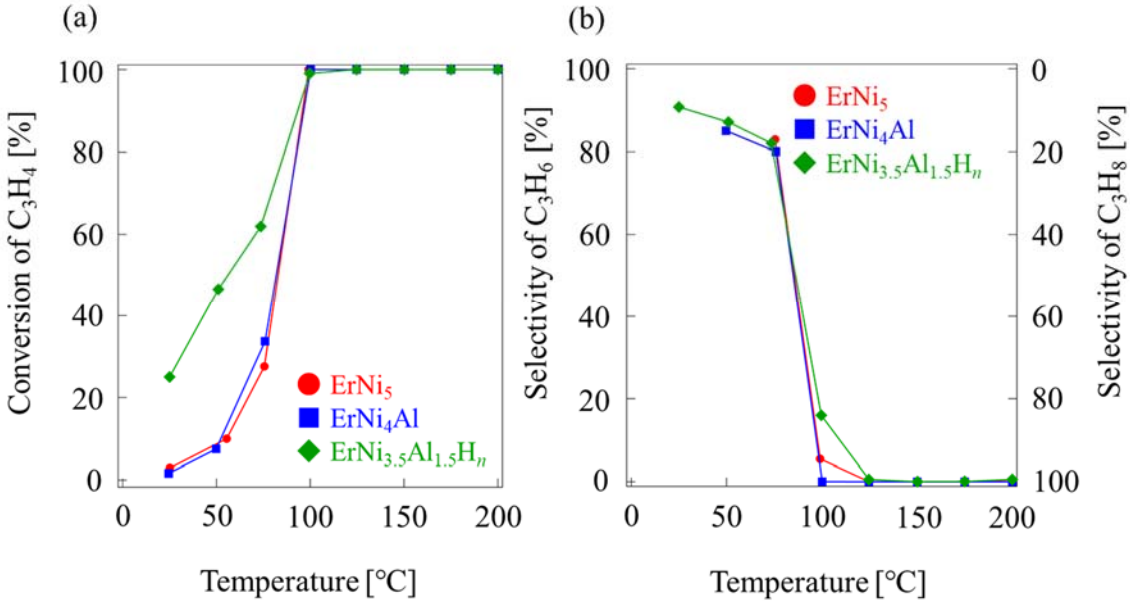

Fig. 7. (a) Conversion of C_3H_4 and (b) selectivity toward C_3H_6 over $ErNi_5$, $ErNi_4Al$, and $ErNi_{3.5}Al_{1.5}$ (reaction gas: 0.4% C_3H_4/19.6% He/80% H_2, total pressure: 0.1 MPa, flow rate: 60 mL min^{-1}).

Table 3 Weight and surface area of each $ErNi_{5-x}Al_x$ alloy in the hydrogenation of C_3H_4

Sample	Weight [g]	Surface area [m^2]
$ErNi_5$	0.2888	0.0259
$ErNi_4Al$	0.3079	0.0257
$ErNi_{3.5}Al_{1.5}H_n$	0.3214	0.0259

3.4 Transient response tests and pulse tests

The absorbed hydrogen may be active for the hydrogenation of C_2H_2. If this is plausible, then hydrogenation can be expected to occur even in a reaction gas flow that does not contain H_2. Transient response tests were performed for $ErNi_5$ (sieved 25–90 μm), $ErNi_{3.5}Al_{1.5}$ (25–90 μm), and $ErNi_{3.5}Al_{1.5}$ (<20 μm) to investigate the contribution of absorbed hydrogen. The results of transient response tests are shown in Fig. 8, and the weight and surface area of each sample are given in Table 4.

$ErNi_5$ (25–90 μm) does not absorb hydrogen under the measurement conditions (P_{H2} = 0.093 MPa), so that improvement due to absorbed hydrogen atoms was not expected. Conversion of C_2H_2 over $ErNi_5$ (25–90 μm) reached less than 20% under a gaseous mixture of C_2H_2 + H_2, and no reaction proceeded under flow of gaseous C_2H_2 + He at any stage [Fig. 8(a)]. Therefore, the H_2 in the gas phase is necessary for hydrogenation and the catalytic reaction does not occur without H_2 supply from the gas phase.

In contrast, for $ErNi_{3.5}Al_{1.5}H_n$ (25–90 μm) with absorbed hydrogen, hydrogenation occurs under a gas flow of C_2H_2 + He that does not contain H_2 [Fig. 8(b)]. These results

indicate that the hydrogenation of C_2H_2 under gaseous C_2H_2+He originates from hydrogen absorbed in bulk $ErNi_{3.5}Al_{1.5}$. The conversion in the second sampling under a gaseous C_2H_2+He flow was lower than that for the first time, which may be due to the consumption of absorbed hydrogen near the surface region between the first and second sampling. $ErNi_{3.5}Al_{1.5}H_n$ (25–90 μm) showed higher reactivity than $ErNi_5$ (25–90 μm) at every reaction stage, as shown in Figs. 8(a) and (b), which is consistent with the results for the hydrogenation of C_2H_2 and C_3H_4 [Figs. 6(a) and 7(a)].

Both $ErNi_5$ (25–90 μm) [Fig. 8(a)] and $ErNi_{3.5}Al_{1.5}H_n$ (25–90 μm) [Fig. 8(b)] show catalytic deterioration with elapse of the reaction time, which is considered to be due to the formation of carbon deposit, such as green oil [35]. Samples are presumed to be easily poised by coking because the surface areas of both samples are small (approximately 0.025 m^2 in Table 4).

Here, we make a comparison between $ErNi_{3.5}Al_{1.5}H_n$ (25–90 μm) and $ErNi_{3.5}Al_{1.5}H_n$ (<20 μm) [Figs. 8(b) and (c)]. The total amount of absorbed hydrogen in the two alloys is almost the same because the weights of the two samples were the same in Table 4. Conversion over $ErNi_{3.5}Al_{1.5}H_n$ (<20 μm) with a flow of gaseous C_2H_2 + H_2 reached 100%, and it was higher than that over $ErNi_{3.5}Al_{1.5}H_n$ (25–90 μm) [Figs. 8(b) and (c)]. This is ascribed to the surface area because the surface area of $ErNi_{3.5}Al_{1.5}H_n$ (<20 μm) was approximately six times larger than that of $ErNi_{3.5}Al_{1.5}H_n$ (25–90 μm) [Table 4]. However, the reactivity over both alloys under a gaseous C_2H_2+He was almost the same at ca. 5–15%, even though the surface area of $ErNi_{3.5}Al_{1.5}$ (<20 μm) is much larger. This negligible effect of surface area under a gaseous C_2H_2+He indicates that the rate-limiting step of the reaction under gaseous C_2H_2+He is hydrogen supply from the bulk alloy because the conversion under gaseous C_2H_2+He increases with

increasing surface area if sufficient hydrogen is supplied from the bulk alloy smoothly. These results also mean that the absorbed hydrogen which reacts with C_2H_2 directly is relatively small (lower than 15% conversion) and hydrogen supply from the gas phase is necessary to achieve an adequate reaction rate. A clean catalyst surface without adsorbed species other than hydrogen is important for the diffusion of hydrogen between the surface and the bulk. Many studies on hydrogen absorption/desorption under a hydrogen atmosphere that contains impurity gases indicate that adsorbed species (O_2 [36-38], CO [36-39], CO_2 [37,38], H_2O [36], and H_2S [38]), even at levels of 50–1000 ppm, can significantly deteriorate the hydrogen absorption/desorption properties, indicating blocking the diffusion of hydrogen between the bulk and surface. Therefore, the low reactivity with only absorbed hydrogen in a flow of 0.7% C_2H_2+He seems to be reasonable.

Pulse tests were conducted with $ErNi_{3.5}Al_{1.5}H_n$ and $ErNi_{3.5}Al_{1.5}$, prepared by different initial treatments to investigate the contribution of absorbed hydrogen in more detail. The results of pulse tests with flowing 2% C_2H_2/18% He/80% H_2 over $ErNi_{3.5}Al_{1.5}H_n$ and $ErNi_{3.5}Al_{1.5}$ are presented in Table 5. The results with flowing 2% C_2H_2/98% He on $ErNi_{3.5}Al_{1.5}H_n$ is shown in Table 6.

Table 5 shows that $ErNi_{3.5}Al_{1.5}H_n$, which was cooled down under hydrogen flow in the pretreatment and possesses absorbed hydrogen, supplies hydrogen to C_2H_2 and produces C_2H_4 with a selectivity of 26.8% with introduction of the first pulse gas (2% C_2H_2/18% He/80% H_2). $ErNi_{3.5}Al_{1.5}H_n$ hydrogenates C_2H_2 with the introduction of the second pulse gas; however, the conversion of C_2H_2 is reduced to almost half and the proportion of C_2H_4 in the products increases up to 52.1%.

$ErNi_{3.5}Al_{1.5}$, which was refrigerated under He flow in the initial treatment and does

not have absorbed hydrogen, showed a completely different result. $ErNi_{3.5}Al_{1.5}$ does not convert C_2H_2 at all, even though an adequate amount of hydrogen (80%) in the pulse gas composition was supplied from the gas phase. These results are the most important in this research. The presence of absorbed hydrogen activates the reactants (C_nH_{2n-2} and hydrogen) from the gas phase and facilitates hydrogenation because the absorbed hydrogen that reacts with C_2H_2 directly is a small quantity, according to the results of transient response tests [Figs. 8(b) and (c)].

As shown in Table 6, the conversion and selectivity over $ErNi_{3.5}Al_{1.5}H_n$ for introduction of the first and second pulse gas mixtures of 2% C_2H_2/98% He were equivalent to that with flowing 2% C_2H_2/18% He/80% H_2 on $ErNi_{3.5}Al_{1.5}H_n$ shown in Table 5, although there is a difference of several percent. These results indicate two factors. Firstly, there is almost no difference in reactivity between hydrogen supplied from the gas phase and the bulk, as long as there is sufficient time to supply adequate hydrogen from the bulk to the surface; i.e., sufficient hydrogen was supplied from the bulk during the initial treatment in a He flow for 10–15 min before introduction of the pulse gas. Therefore, $ErNi_{3.5}Al_{1.5}H_n$ shows the same reactivity with 2% C_2H_2/98% He as that with 2% C_2H_2/18% He/80% H_2. However, the reactivity was relatively low in the transient response test, in which C_2H_2 was supplied continually [Figs. 8(b) and (c)] because the hydrogen supply became the rate-limiting step for the reaction. Secondly, these results guarantee that ample hydrogen is present in bulk $ErNi_{3.5}Al_{1.5}$ even in the transient response tests under gaseous C_2H_2+He [Figs. 8(b) and (c)] because there was sufficient activity toward 2% C_2H_2/98% He over $ErNi_{3.5}Al_{1.5}H_n$ in the pulse test after being kept under He flow for 10 to 25 min.

We conclude that the role of absorbed hydrogen is to activate C_nH_{2n-2} and hydrogen,

and to accelerate the reaction, as revealed by transient response tests and pulse tests. The difference of electronic states between $ErNi_{3.5}Al_{1.5}H_n$ and $ErNi_{3.5}Al_{1.5}$ could influence the catalytic property. Aleksandrov et. al. reported that the subsurface hydrogen of Pd destabilizes the adsorbed hydrogen on Pd surface due to changing the electronic structure of Pd [22]. They explained that the Pd 4d band shifts toward lower energies with the subsurface hydrogen, and the antibonding states between the adsorbed hydrogen (1s) and Pd (4d) also move below the Fermi level simultaneously. The occupation of the antibonding states weakens hydrogen adsorption on the Pd surface. [22]. Consequently, the weak adsorbed hydrogen is activated and accelerates hydrogenation reaction in the case of Pd catalyst [22]. The catalytic activity of $ErNi_{3.5}Al_{1.5}H_n$ might be improved by the similar mechanism. On the other hand, the previous report on the hydrogenation of C_2H_4 on $LaNi_5H_n$ suggests that hydrogenation occurs using absorbed hydrogen and not by gas phase hydrogen because the dual sites that are necessary for gaseous hydrogen adsorption could be lost by adsorbed C_2H_4, which covers most of the surface [24]. That study was conducted using a gas circulation system and the reaction temperature range was very low, from -60 °C to -84 °C. The contribution of absorbed hydrogen is considered to be influenced by the measurement temperature. Furthermore, the well-known hydrogen storage alloy, Mg_2Ni, decreases the reactivity toward the hydrogenation of C_2H_2 by the formation of the hydride, Mg_2NiH_4 [29]. More detailed study regarding hydrogen storage alloys and their catalysts is desired with respect to characteristics such as the measurement temperature range, electronic state, crystal structure, and the interaction between absorbed hydrogen and alloy.

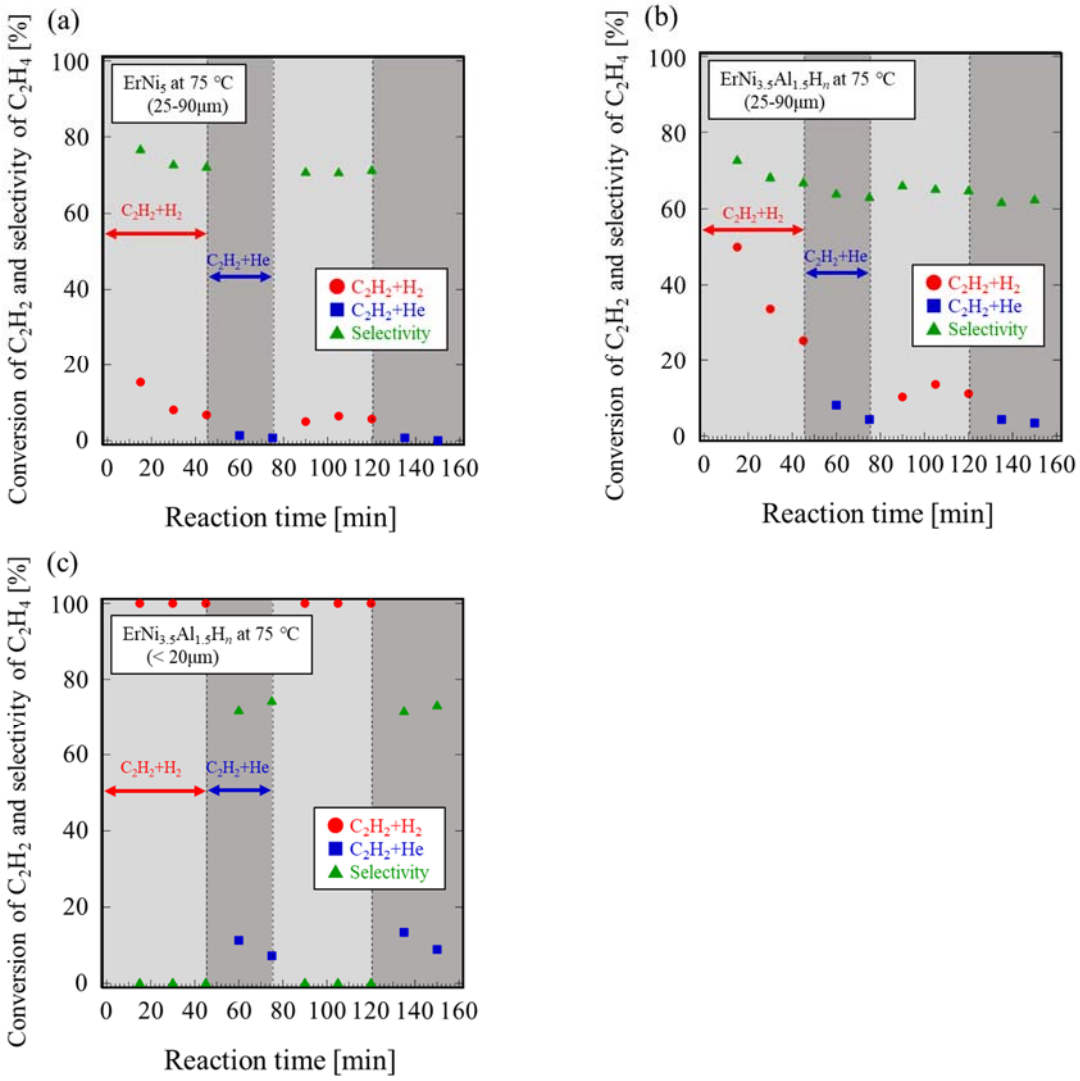

Fig. 8. Transient response results; (a) $ErNi_5$ (sieved in the range of 25–90 μm), (b) $ErNi_{3.5}Al_{1.5}$ (25–90 μm), (c) $ErNi_{3.5}Al_{1.5}$ (<20 μm) (Reaction gas: 0.7% C_2H_2/6% He/93.3% H_2 or 0.7% C_2H_2/99.3% He, total pressure: 0.1 MPa, flow rate: 30 mL min^{-1}).

Table 4 Weight and surface area of each $ErNi_{5-x}Al_x$ alloy in the transient response tests

Sample (particle size)	Weight [g]	Surface area [m^2]
(a) $ErNi_5$ (25-90 μm)	0.3031	0.027
(b) $ErNi_{3.5}Al_{1.5}H_n$ (25-90 μm)	0.3216	0.026
(c) $ErNi_{3.5}Al_{1.5}H_n$ (< 20 μm)	0.3278	0.154

Table 5 Conversion of C_2H_2 and selectivity toward C_2H_4 over $ErNi_{3.5}Al_{1.5}H_n$ and $ErNi_{3.5}Al_{1.5}$ in pulse tests with flowing 2% C_2H_2/18% He/80% H_2 at 25 °C

Sample	Conversion of C_2H_2 in 1st pulse	Selectivity of C_2H_4 in 1st pulse	Conversion of C_2H_2 in 2nd pulse	Selectivity of C_2H_4 in 2nd pulse
$ErNi_{3.5}Al_{1.5}H_n$	83.5 % (±7.3)	26.8 % (±10.3)	43.0 % (±7.4)	52.1 % (±0.6)
$ErNi_{3.5}Al_{1.5}$	Not detected	-	Not detected	-

Table 6 Conversion of C_2H_2 and selectivity toward C_2H_4 over $ErNi_{3.5}Al_{1.5}H_n$ in pulse tests with flowing 2% C_2H_2/98% He at 25 °C

Sample	Conversion of C_2H_2 in 1st pulse	Selectivity of C_2H_4 in 1st pulse	Conversion of C_2H_2 in 2nd pulse	Selectivity of C_2H_4 in 2nd pulse
$ErNi_{3.5}Al_{1.5}H_n$	70.5 % (±7.3)	39.8 % (±3.2)	36.2 % (±7.2)	53.6 % (±2.0)

Conclusion

XRD studies and Rietveld analysis of the $ErNi_{5-x}Al_x$ (x=0, 0.5, 0.75, 1, 1.25, and 1.5) alloys indicated that Al atoms substitute for Ni atoms at 3g sites without changing the hexagonal structure ($CaCu_5$-type) with the space group P6/mmm. The lattice volume expanded linearly with an increase of the Al content.

The hydrogen storage properties of the $ErNi_{5-x}Al_x$ (x=0, 0.5, 0.75, 1, 1.25, and 1.5) alloys were investigated at temperatures higher than 25 °C by PCI and *in situ* XRD measurements under a hydrogen atmosphere. These alloys absorbed hydrogen at lower hydrogen pressures with an increase of the Al content because the replacement of Ni with Al created larger interstitial spaces.

In catalytic tests, $ErNi_{3.5}Al_{1.5}H_n$ with absorbed hydrogen showed higher activity

for the hydrogenation of C_2H_2 and C_3H_4 than $ErNi_5$ and $ErNi_4Al$ without absorbed hydrogen. The contribution of absorbed hydrogen to the hydrogenation reaction was discussed with the results of transient response tests and pulse tests. The absorbed hydrogen reacts with C_2H_2 directly under C_2H_2+He flow in transient response tests, although the amount was relatively small because the hydrogen supply from the bulk is the rate-limiting step under a constant C_2H_2 flow.

Pulse tests were conducted with $ErNi_{3.5}Al_{1.5}H_n$ and $ErNi_{3.5}Al_{1.5}$ prepared using different initial treatments. $ErNi_{3.5}Al_{1.5}H_n$ with absorbed hydrogen showed catalytic reactivity with supplied 2% C_2H_2/18% He/80% H_2. However, $ErNi_{3.5}Al_{1.5}$ without absorbed hydrogen did not convert C_2H_2 at all, even though the reaction gas contained adequate hydrogen. According to transient response tests and pulse tests, the role of absorbed hydrogen for the hydrogenation of C_nH_{2n-2}, absorbed hydrogen activates adsorbates (C_nH_{2n-2} and hydrogen) that are supplied from the gas phase.

Acknowledgment

This work was supported financially by Grants-in-Aid for Scientific Research ((B) 18H01783, 19H02452) from the Ministry of Education, Culture, Sports, Science and Technology (MEXT) of Japan and "Dynamic Alliance for Open Innovation Bridging Human, Environment and Materials".

References

[1] Sakintuna B, Lamari-Darkrim F, Hirscher M. Metal hydride materials for solid hydrogen storage: A review. Int J Hydrogen Energy 2007;32:1121-40 and references

therein.

[2] Jain IP, Lal C, Jain A. Hydrogen storage in Mg: A most promising material. Int J Hydrogen Energy 2010;35:5133-44

[3] Bououdina M, Grant D, Walker G. Review on hydrogen absorbing materials—structure, microstructure, and thermodynamic properties. Int J Hydrogen Energy 2006;31:177-82

[4] Van Vucht JHN, Kuijpers FA, Bruning HCAM. Reversible room-temperature absorption of large quantities of hydrogen by intermetallic compounds. Philips Res Rep 1970;25:133-40.

[5] Mendelsohn MH, Gruen DM, Dwight AE. $LaNi_{5-x}Al_x$ is a versatile alloy system for metal hydride applications. Nature 1977;269:45-7.

[6] Diaz H, Percheron-Guégan A, Achard JC, Chatillon C, Mathieu JC. Thermodynamic and structural properties of $LaNi_{5-y}Al_y$ compounds and their related hydrides. Int J Hydrogen Energy. 1979;4:445-54.

[7] Yamagishi R, Kojima T, Kameoka S, Okuyama D, Sato TJ, Nishimura C, Tsai AP. Creating the hydrogen absorption capability of $CeNi_5$ through the addition of Al. Int J Hydrogen Energy 2017;42:21832-40.

[8] Šorgić B, Blažina Ž, Drašner A. A study of structural and thermodynamic properties of the $YNi_{5-x}Al_x$-hydrogen system. J Alloys Comp 1998;265:185-9.

[9] Bobet J-L, Pechev S, Chevalier B, Darriet B. Structural and hydrogen sorption studies of $NdNi_{5-x}Al_x$ and $GdNi_{5-x}Al_x$. J Alloys Comp 1998;267:136-41.

[10] Biliškov N, Miletić GI, Drašner A, Prezelj K. Structural and hydrogen sorption properties of $SmNi_{5-x}Al_x$ system - An experimental and theoretical study. Int J Hydrogen Energy 2015;40:8548-61.

[11] Blažina Ž, Šorgić B, Drašner A. The crystal structure and some thermodynamic properties of the $TbNi_{5-x}Al_x$-hydrogen system. J Phys Condens Matter 1997;9:3099-105.

[12] Šorgić B, Drašner A, Blažina Ž. On the structural and thermodynamic properties of the $DyNi_{5-x}Al_x$-hydrogen system. J Phys Condens Matter 1995;7:7209-15.

[13] Blažina Ž, Šorgić B, Drašner A. On some structural and hydrogen sorption properties of the $HoNi_{5-x}Al_x$ intermetallics. J Mater Sci Lett 1997;16:1683-5.

[14] Šorgić B, Drašner A, Blažina Ž. The effect of aluminium on the structural and hydrogen sorption properties of $ErNi_5$. J Alloys Comp 1996;232:79-83.

[15] Takeshita T, Malik SK, Wallace WE. Hydrogen absorption in RNi_4Al (R=Rare Earth) ternary compounds. J Solid State Chem 1978;23:271-4.

[16] Doyle AM, Shaikhutdinov SK, Jackson SD, Freund HJ. Hydrogenation on metal surfaces: Why are nanoparticles more active than single crystals?. Angew Chem Int Ed 2003;42:5240-3.

[17] Morkel M, Rupprechter G, Freund HJ. Finite size effects on supported Pd nanoparticles: Interaction of hydrogen with CO and C_2H_4. Surf Sci 2005;588:L209-L19.

[18] Doyle AM, Shaikhutdinov SK, Freund HJ. Alkene chemistry on the palladium surface: nanoparticles vs. single crystals. J Catal 2004;223:444-53.

[19] Wilde M, Fukutani K, Ludwig W, Brandt B, Fischer JH, Schauermann S, Freund HJ. Influence of carbon deposition on the hydrogen distribution in Pd nanoparticles and their reactivity in olefin hydrogenation. Angew Chem Int Ed 2008;47:9289-93.

[20] Teschner D, Borsodi J, Wootsch A, Révay Z, Hävecker M, Knop-Gericke A, Jackson SD, Schlögl R. The roles of subsurface carbon and hydrogen in palladium-catalyzed alkyne hydrogenation. Science 2008;320:86-9.

[21] Ludwig W, Savara A, Schauermann S, Freund HJ. Role of low-coordinated surface sites in olefin hydrogenation: A molecular beam study on Pd nanoparticles and Pd(111). ChemPhysChem 2010;11:2319-22.

[22] Aleksandrov HA, Kozlov SM, Schauermann S, Vayssilov GN, Neyman KM. How

absorbed hydrogen affects the catalytic activity of transition metals. Angew Chem Int Ed 2014;53:13371-13375.

[23] Ohno S, Wilde M, Mukai K, Yoshinobu J, Fukutani K. Mechanism of olefin hydrogenation catalysis driven by palladium dissolved hydrogen. J Phys Chem C 2016;120:11481-9.

[24] Soga K, Imamura H, Ikeda S. Hydrogenation of ethylene over $LaNi_5$ Alloy. J Phys Chem 1977;81:1762-6.

[25] Soga K, Otsuka K, Sato M, Sano T, Ikeda S. Hydrogenation of ethylene over an $LaNi_5$ plate. J Less-Common Met 1980;71:259-63.

[26] Soga K, Imamura H, Ikeda S. Hydrogenation of ethylene over some intermetallic compounds. J Catal 1979;56:119-26.

[27] Kato S, Borgschulte A, Ferri D, Bielmann M, Crivello CJ, Wiedenmann D, Parlinska-Wojtan M, Rossbach P, Lu Y, Remhof A, Züttel A. CO_2 hydrogenation on a metal hydride surface. Phys Chem Chem Phys 2012;14:5518-26.

[28] Kato S, Matam SK, Kerger P, Bernard L, Battaglia C, Vogel D, Rohwerder M, Züttel A. The origin of the catalytic activity of a metal hydride in CO_2 reduction. Angew Chem Int Ed 55 2016;55:6028-32.

[29] Tsukuda R, Yamagishi R, Kameoka S, Nishimura C, Tsai AP. Ability of hydrogen storage $CeNi_{5-x}Ga_x$ and Mg_2Ni alloys to hydrogenate acetylene. Sci Technol Adv Mater 2019;20:774-85.

[30] Rodríguez-Carvajal J. Recent developments of the Program FULLPROF. In CPD Newsletter 2001;12:26; available at http://www.ill.eu/sites/fullprof/index.html

[31] Wernick JH, Geller S. Transition element-rare earth compounds with Cu_5Ca structure. Acta Crystallogr 1959;12:662-5.

[32] Buschow KHJ. Crystal structures, magnetic properties and phase relations of erbium-nickel intermetallic compounds. J Less-Common Met 1968;16:45-53.

[33] Percheron-Guégan A, Lartigue C, Achard JC, Germi P, Tasset F. Neutron and X-ray diffraction profile analyses and structure of $LaNi_5$, $LaNi_{5-x}Al_x$, $LaNi_{5-x}Mn_x$, intermetallics and their hydride (deuteride). J Less-Common Met 1980;74:1-12.

[34] Du H, Zhang W, Wang C, Han J, Yanga Y, Chen B, Xie C, Sun K, Zhang B. Neutron powder diffraction study on the structures of $LaNi_{5-x}Al_xD_y$ compounds. Solid State Commun 2003;128:157-61.

[35] Bos ANR, Westerterp KR. Mechanism and kinetics of the selective hydrogenation of ethyne and ethane. Chem Eng Process 32 1993;32:1-7.

[36] Sandrock GD, Goodell PD. Surface poisoning of $LaNi_5$ and (Fe, Mn)Ti by O_2, CO and H_2O. J Less-Common Met 1980;73:161-8.

[37] Hirata T. Hydrogen absorption and desorption properties of $FeTi_{1.14}O_{0.03}$ in impure hydrogen containing CO, CO_2 and oxygen. J Less-Common Met 1985;107:23-33.

[38] Schweppe F, Martin M, Fromm E. Hydrogen absorption of $LaNi_5$ powders precovered with O_2, CO, H_2S, CO_2 or N_2. J Alloys Comp 1997;253/254:511-4.

[39] Han S, Zhang X, Shi S, Tanaka H, Kuriyama N, Taoka N, Aihara K, Xu Q. Experimental and theoretical investigation of the cyclic durability against CO and degradation mechanism of the $LaNi_5$ hydrogen storage alloy. J Alloys Comp 2007;446/447:208-11.